A RANDOM MATRIX MODEL FOR mmWAVE MIMO SYSTEMS*

G. Alfano, C.-F. Chiasserini, A. Nordio, D.G. Riviello

Politecnico di Torino
Corso Duca degli Abruzzi 24, 10129 Torino, Italy

(Received December 25, 2019)

Random matrices are nowadays classical tools for modeling multiantenna wireless channels. Scattering phenomena typical of cellular frequencies and channel reciprocity features led to the adoption of matrices sampled either from the Gaussian Unitary Ensemble (GUE) or from more general Polynomial Ensembles (PE). Such matrices can be used to model the random impairments of the radio channel on the transmitted signal over a wireless link whose transmitter and receiver are both equipped with antenna arrays. The exploitation of the millimeter-wave (mmWave) frequency band, planned for 5G and beyond mobile networks, prevents the use of GUE and PE elements as candidate models for channel matrices. This is mainly due to the lack of scattering richness compared to microwave-based transmissions. In this work, we propose to model mmWave Multi-Input–Multi-Output (MIMO) systems via products of random Vandermonde matrices. We illustrate the physical motivation of our model selection, discuss the meaning of the parameters and their impact on the spectral properties of the random matrix at hand, and provide both a list of results of immediate use for performance analysis of mmWave MIMO systems, as well as a list of open problems in the field.

DOI:10.5506/APhysPolB.51.1627

1. Introduction

Random matrix theory has been introduced as a mathematical tool for modeling and analysis of wireless multiantenna communications since the earliest stages of development and prototyping of such a technology [1]. A fully detailed model of a point-to-point link between a transmitter and a receiver both equipped with linear antenna arrays requires the characterization of a product of random matrices whose entries are function of not

* Presented at the conference *Random Matrix Theory: Applications in the Information Era*, Kraków, Poland, April 29–May 3, 2019.

necessarily independent random variables, tied up to the scattering phenomena typical of the exploited cellular frequencies [2]. However, most of the practical scenarios of interest have been successfully analyzed relying on reasonable simplifications of the channel dynamics [3–6], leading to the adoption of matrices sampled either from the GUE or from PE as channel matrices. Indeed, more sophisticated transmission schemes, featuring relay-aided and network-encoded ones, have been adequately modeled in the multiantenna setting by means of sums and products of random matrices from the mentioned ensembles (see *e.g.* [7, 8]). Therefore, analytical performance analysis and compact design guidelines discussion have been possible by virtue of the availability of explicit expressions for the spectral statistics of the involved channel matrices.

However, starting from 5G, the use of mmWave frequencies is planned: thanks to the large bandwidth available in the 30–300 GHz spectrum, mmWave has imposed itself as one of the main enablers for ultra-broadband communications. Nonetheless, such a technology poses some serious hurdles that need to be overcome. First, and more prominently, the high attenuation to which mmWave communications are prone [9], which requires the use of large antenna arrays (made possible by the small wavelength, hence the small elements size) and directional beamforming. Second, it has been observed that a mmWave channel is characterized by few strong paths, along which it is essential that both the access node and the user terminal align their beams [10].

The need for modeling such propagation phenomena and technical strategies prevents the use of GUE and PE elements as channel matrices, thus a good candidate model is still missing. Such a model should encompass the main features of a signal transmission taking place in the mentioned frequency band, on top of all poor scattering and blocking effects due to the different ratio between the wavelength of interest and the size of objects of daily use.

In this work, we propose to model mmWave MIMO systems via products of random Vandermonde matrices. We illustrate the physical motivation of our model selection, discuss the meaning of the parameters and their impact on the spectral properties of the random matrix at hand. We also provide a list of existing results of immediate use for basic performance analysis of mmWave MIMO systems, as well as a list of array geometries of interest, for which the adoption of generalized[1] Vandermonde models would provide a suitable analytical channel representation.

[1] By generalized Vandermonde matrices, we refer to the random matrix models reported in [11, Sec. III.D].

2. System model

We focus on a point-to-point MIMO communication system where the transmitter and the receiver are equipped with N_{T} and N_{R} antennas, respectively. At each signaling interval, the communication is described by the input–output relationship

$$\boldsymbol{y} = \boldsymbol{H}\boldsymbol{x} + \boldsymbol{n}\,, \tag{1}$$

where

— $\boldsymbol{x}$ is a random vector of size N_{T} and covariance $\mathbb{E}[\boldsymbol{x}\boldsymbol{x}^{\mathsf{H}}] = \frac{\mathcal{E}_s}{N_{\mathrm{T}}}\boldsymbol{I}$, representing the information that the transmitter sends to the receiver;

— $\boldsymbol{H}$ is the $N_{\mathrm{R}} \times N_{\mathrm{T}}$ random channel matrix;

— $\boldsymbol{y}$ is the received signal vector of length N_{R}, and

— $\boldsymbol{n}$ represents additive Gaussian noise with covariance $\mathbb{E}[\boldsymbol{n}\boldsymbol{n}^{\mathsf{H}}] = N_0\boldsymbol{I}$.

In general, the statistics of the channel matrix deeply affect the performance of the communication system. In the literature, several channel models have been analyzed, taking into account important geometric and system parameters, such as the carrier frequency, the presence or absence of reflecting obstacles, and the movement of both the transmitter and the receiver. In our work, we consider the channel model in [12, Eq. (3)] which is well-suited for mmWave communications and for the case where the antennas at both the transmitter and the receiver are organized in a uniform linear array (ULA). This model is an extension to the Saleh–Valenzuela geometric model [13] and the matrix $\boldsymbol{H}$ is given by[2]

$$\boldsymbol{H} = \sqrt{\frac{N_{\mathrm{T}}\,N_{\mathrm{R}}}{L}} \sum_{\ell=1}^{L} \alpha_\ell \boldsymbol{u}_\ell \boldsymbol{v}_\ell^{\mathsf{H}} = \mathsf{g}\boldsymbol{U}\boldsymbol{D}\boldsymbol{V}^{\mathsf{H}}\,. \tag{2}$$

Equation (2) describes a propagation environment where the signal is scattered by L clusters/paths with no near-field impairments at the receiver. The term $\mathsf{g} = \sqrt{\frac{N_{\mathrm{T}}\,N_{\mathrm{R}}}{L}}$ accounts for the normalization of the channel energy, $\boldsymbol{U} = [\boldsymbol{u}_1, \ldots, \boldsymbol{u}_L]$ is a matrix of size $N_{\mathrm{R}} \times L$, $\boldsymbol{V} = [\boldsymbol{v}_1, \ldots, \boldsymbol{v}_L]$ has size $N_{\mathrm{T}} \times L$, and $\boldsymbol{D} = \mathrm{diag}(\alpha_1, \ldots, \alpha_L)$. Following [12], we assume the coefficients α_ℓ to be i.i.d. complex random variables with zero-mean and

[2] The model described hereinafter has already been exploited in [14], where the emphasis is on the performance of practical transmission strategies, leading to the analysis of a reduced-rank version of the random matrix product we focus on throughout our work.

unit variance. Furthermore, $\boldsymbol{u}_\ell$ and $\boldsymbol{v}_\ell$ represent the transmit and receive steering vectors corresponding to the ℓ^{th} path. If the transmit and receive antennas are ULAs, then

$$\begin{aligned} \boldsymbol{u}_\ell &= \sqrt{\frac{1}{N_{\text{R}}}}\left[1, \mathrm{e}^{\mathrm{j}kd_{\text{R}}\cos(\phi_{\text{R},\ell})}, \ldots, \mathrm{e}^{\mathrm{j}(N_{\text{R}}-1)kd_{\text{R}}\cos(\phi_{\text{R},\ell})}\right]^{\mathsf{T}}, \\ \boldsymbol{v}_\ell &= \sqrt{\frac{1}{N_{\text{T}}}}\left[1, \mathrm{e}^{\mathrm{j}kd_{\text{T}}\cos(\phi_{\text{T},\ell})}, \ldots, \mathrm{e}^{\mathrm{j}(N_{\text{T}}-1)kd_{\text{T}}\cos(\phi_{\text{T},\ell})}\right]^{\mathsf{T}}, \end{aligned} \tag{3}$$

where d_{T} and d_{R} denote the distances between adjacent transmit and receive antenna elements, respectively, $k = 2\pi/\lambda$, $\phi_{\text{R},\ell}$ is the Angle of Arrival from the ℓ^{th} propagation cluster, and $\phi_{\text{T},\ell}$ is the Angle of Departure to the ℓ^{th} propagation cluster. We assume the angles $\phi_{\text{R},\ell}$ and $\phi_{\text{T},\ell}$, $\ell = 1, \ldots, L$ to be i.i.d. random variables with probability density functions (p.d.f.) symmetric around their mean, as done in [15, Table I] and [16]. Although the angles $\phi_{\text{T},\ell}$, $\ell = 1, \ldots, L$ can be considered as i.i.d. random variables, for every ℓ, the angle $\phi_{\text{R},\ell}$ could be strongly correlated to $\phi_{\text{T},\ell}$. Such a correlation depends on the geometry of the problem and on the ULAs orientations. Therefore, in general, the Vandermonde matrices $\boldsymbol{U}$ and $\boldsymbol{V}$ are not independent.

3. Channel matrix statistics

Under our assumptions, both $\boldsymbol{U}$ as well as $\boldsymbol{V}$ are, disregarding the normalization factors $\sqrt{\frac{1}{N_{\text{R}}}}$ and $\sqrt{\frac{1}{N_{\text{T}}}}$, random Vandermonde matrices with entries lying on the unit circle [11, Eq.(1)], and *phases* given by $\omega_{\text{R},\ell} = kd_{\text{R}}\cos(\phi_{\text{R},\ell})$ and by $\omega_{\text{T},\ell} = kd_{\text{T}}\cos(\phi_{\text{T},\ell})$, respectively.

The statistical properties of the matrix $\boldsymbol{H}^{\mathsf{H}}\boldsymbol{H}$ are known to dictate the ultimate (information-theoretic) performance of MIMO systems [3, and references therein]. Therefore, hereinafter we summarize results from the literature on random Vandermonde matrices, which will be useful in the remainder of the paper. Currently, a tractable analysis of random matrices whose columns have the structure in (3) is only available when both $N_{\text{R}}, N_{\text{T}}$ and L grow large at the same rate, *i.e.*, when the ratios N_{R}/L and N_{T}/L asymptotically tend to positive, finite values. Most of our analysis will assume instead that the number of antennas at both the transmitter and the receiver, as well as the number of paths, are finite.

3.1. Moments and eigenvalues

Let $\boldsymbol{A}$ be a (properly normalized) $N \times M$ random matrix and let $\lambda_1, \ldots, \lambda_M$ be the random eigenvalues of $\boldsymbol{A}^{\mathsf{H}}\boldsymbol{A}$. Then, the n^{th} asymptotic moment of $\boldsymbol{A}$ is defined as

$$A_n = \lim \mathbb{E}\left[\frac{1}{M}\mathsf{Tr}\left\{\left(\boldsymbol{A}^{\mathsf{H}}\boldsymbol{A}\right)^n\right\}\right] = \int \lambda^n f_{\boldsymbol{A}}(\lambda)\,\mathrm{d}\lambda \tag{4}$$

whenever the limit exists. In (4), the limit is computed by assuming that $N, M \to \infty$ while the ratio N/M is kept finite. Moreover, $f_{\boldsymbol{A}}(\cdot)$ is the limiting spectral distribution of $\boldsymbol{A}^{\mathsf{H}}\boldsymbol{A}$. The expression for $f_{\boldsymbol{A}}(\cdot)$ depends on the distribution and on the correlation between the entries of $\boldsymbol{A}$.

When $\boldsymbol{A}$ is a random Vandermonde matrix whose columns are as in (3), a closed-form expression for $f_{\boldsymbol{A}}(\lambda)$ is still unknown. However, the expression of the moments in (4), which depend on the distribution of the phases ω, can be obtained as described in [11, Theorem I] and in [17–19]. In general, the existence of all the moments in (4) is not sufficient to guarantee the existence of a limiting probability measure having these moments. Nevertheless, for random Vandermonde matrices, the convergence of the empirical eigenvalue distribution to a limiting probability measure, supported on $[0, +\infty)$, has been proven in [20].

In the case of mmWave links, the channel matrix $\boldsymbol{H}$ in (2) is given by a mixed product of two random Vandermonde matrices and a random diagonal matrix. Therefore, the computation of its moments is more challenging than that of a single Vandermonde matrix. In our scenario, the n^{th} asymptotic moment of $\boldsymbol{H}^{\mathsf{H}}\boldsymbol{H}$, H_n, can be computed as

$$\begin{aligned} H_n &= \lim \mathbb{E}\left[\frac{1}{N_{\mathrm{T}}}\mathsf{Tr}\left\{\left(\frac{1}{L}\boldsymbol{H}^{\mathsf{H}}\boldsymbol{H}\right)^n\right\}\right] \\ &= \lim \mathsf{g}^{2n}\mathbb{E}\left[\frac{1}{N_{\mathrm{T}}}\mathsf{Tr}\left\{\left(\frac{1}{L}\boldsymbol{V}\boldsymbol{D}^{\mathsf{H}}\boldsymbol{U}^{\mathsf{H}}\boldsymbol{U}\boldsymbol{D}\boldsymbol{V}^{\mathsf{H}}\right)^n\right\}\right] \\ &= \lim \frac{N_{\mathrm{T}}^{n-1}N_{\mathrm{R}}^n}{L^n}\mathbb{E}\left[\mathsf{Tr}\left\{\left(\boldsymbol{D}^{\mathsf{H}}\boldsymbol{U}^{\mathsf{H}}\boldsymbol{U}\boldsymbol{D}\boldsymbol{V}^{\mathsf{H}}\boldsymbol{V}\right)^n\right\}\right], \end{aligned} \tag{5}$$

where the limit is computed by assuming that $N_{\mathrm{T}}, N_{\mathrm{R}}, L \to \infty$, while the ratios N_{T}/L and N_{R}/L are kept finite. The term $\frac{1}{L}$ appearing in (5) is a normalization factor ensuring the convergence of the limit. Histograms of the limiting eigenvalue distribution of our channel matrix in both cases of scalar and Gaussian $\boldsymbol{D}$ are depicted in figure 1.

A combinatorial description of the mixed moments of independent Vandermonde matrices and diagonal matrices appears in [11, Theorem 7], which provides expressions of the form of

$$\lim \frac{1}{L}\mathbb{E}\left[\mathsf{Tr}\left\{\boldsymbol{D}_1\boldsymbol{V}_{i_1}^{\mathsf{H}}\boldsymbol{V}_{i_2}\boldsymbol{D}_2\boldsymbol{V}_{i_2}^{\mathsf{H}}\boldsymbol{V}_{i_3}\cdots\boldsymbol{D}_n\boldsymbol{V}_{i_n}^{\mathsf{H}}\boldsymbol{V}_{i_1}\right\}\right], \tag{6}$$

where $\{i_1, \ldots, i_n\} \in \{1, \ldots, n\}$. However, equations (5) and (6) differ under many aspects. First of all, in [11, Theorem 7] all the considered Vandermonde matrices are independent of each other and have the same size, while

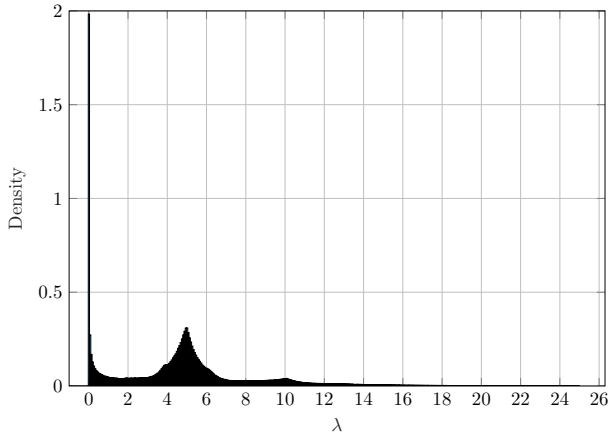

(a) $\boldsymbol{D} = \boldsymbol{I}$ [11].

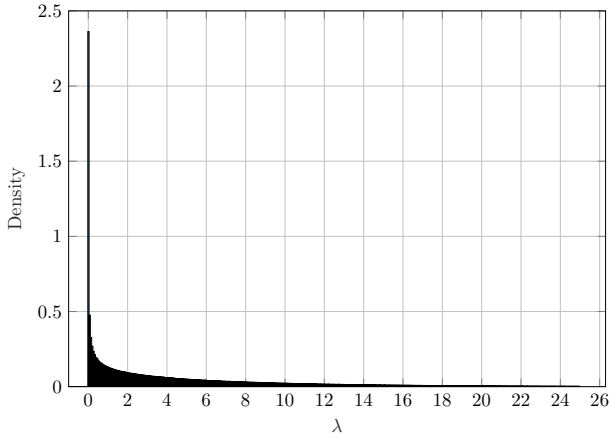

(b) Gaussian case, $\boldsymbol{D} = \mathrm{diag}(\alpha_1, \ldots, \alpha_L)$ with $\alpha_\ell \sim \mathcal{CN}(0, \mathbf{I})$.

Fig. 1. Spectral density of $\boldsymbol{H}^{\mathsf{H}}\boldsymbol{H}$.

in (5) the matrices $\boldsymbol{U}$ and $\boldsymbol{V}$ may be correlated and have a different number of rows. Moreover, (6) considers the more general case where n random diagonal matrices are available, while in our case, we have a single matrix $\boldsymbol{D}$.

In the non-asymptotic case, *i.e.*, when the size of the involved matrices is finite, we are interested in the evaluation of the following expression:

$$\mathbb{E}\left[\mathsf{Tr}\left(\boldsymbol{H}^{\mathsf{H}}\boldsymbol{H}\right)^n\right] = \sum_{\boldsymbol{\ell},\boldsymbol{k}} \mathbb{E}\left[\alpha_{\ell_1}\alpha_{k_1}^* \ldots \alpha_{\ell_n}\alpha_{k_n}^*\right] \mathbb{E}\left[\left(\boldsymbol{V}^{\mathsf{H}}\boldsymbol{V}\right)_{\ell_1,k_1} \ldots \left(\boldsymbol{V}^{\mathsf{H}}\boldsymbol{V}\right)_{\ell_n,k_n}\right] \times \mathbb{E}\left[\left(\boldsymbol{U}^{\mathsf{H}}\boldsymbol{U}\right)_{\ell_1,k_1} \ldots \left(\boldsymbol{U}^{\mathsf{H}}\boldsymbol{U}\right)_{\ell_n,k_n}\right], \tag{7}$$

where the expectation factorizes by virtue of the independence among the factors in (2). The sum in (7) is over the vectors of integers $\boldsymbol{\ell} = [\ell_1, \ldots, \ell_n]$

and $\boldsymbol{k} = [k_1, \ldots, k_n]$, where $\ell_j, k_j \in \{1, \ldots, L\}$, and $j = 1, \ldots, n$. Our assumptions on the elements of the matrix $\boldsymbol{D}$, allow us to simplify the above expression by applying Wick's formula [21].

To conclude our discussion on the spectral statistics of the mixed product of Vandermonde and diagonal matrices, we recall that the spectrum of the channel matrix $\boldsymbol{H}$ is expected to have an unbounded support according to the results reported in [22, Sec.VI]. In particular, the largest eigenvalue of $\boldsymbol{H}^{\mathsf{H}}\boldsymbol{H}$ is expected to scale with the matrix size.

Regarding the smallest eigenvalue of $\boldsymbol{H}^{\mathsf{H}}\boldsymbol{H}$, an estimation of the probability mass in zero can be obtained according to what reported in [22, Sec.VI]. Numerical investigation on the spectral support of the matrix $\boldsymbol{H}^{\mathsf{H}}\boldsymbol{H}$, as well as an analytical study of bounds on its largest eigenvalue, are still subject of ongoing work.

3.2. Discussion on the application of free probability

Random Vandermonde matrix models considered in [11] and mixed products as per (2) can be studied with the help of a recent extension of the free probability, the so-called traffic-freeness [25]. Such a theory applies to random matrices whose distribution is invariant under unitary transformations given by random permutation matrices. Otherwise stated, traffic-freeness extends to permutation-invariant random matrices some of the results available for Haar-invariant random matrices. Explicit reference to mixed products of random Vandermonde and deterministic matrices is made in [23, 24], but none of the available works deal with the case of mixed products of independent Vandermonde matrices. A promising research direction is constituted by the extension of the results in [24] to matrix products of the type in (2). Furthermore, we believe that exploiting a link between mmWave MIMO models and the theory of asymptotic liberation [26][3] could lead to an advancement in establishing analytical machineries and tools providing more compact results on 5G-and-beyond communication.

4. Mutual information statistics

Let us assume that full channel state information (CSI) (*i.e.*, the matrix $\boldsymbol{H}$) is available at the receiver, while the transmitter has no access to CSI and allocates the available input power uniformly across the transmit antennas. Under these assumptions, the ergodic capacity of the MIMO channel (1) is given by

[3] Our conjecture stems from the fact that asymptotic liberation theory has already turned helpful in the study of mixed products of Fourier matrices appearing in doubly-selective fading scenarios (see [26, 27]).

$$C(\gamma) = \mathbb{E}\left[\log\left|\boldsymbol{I} + \gamma \boldsymbol{H}^{\mathsf{H}}\boldsymbol{H}\right|\right], \tag{8}$$

where $\gamma = \mathcal{E}_s/(N_{\mathrm{T}}\, N_0)$. Since a closed-form expression for (8) is still unknown, we separately investigate the behavior of the ergodic capacity in two extreme SNR regimes, namely for very low and very high values of γ, and summarize the findings in the next subsections.

4.1. Low-power regime

For low values of the input power, the spectral efficiency of a MIMO channel is easier to analyze w.r.t. the corresponding capacity. Such spectral efficiency can be expressed in terms of the value of transmitted energy per-bit $\mathcal{E}_{\mathrm{b}}/N_0$, *i.e.*,

$$\mathsf{C}\left(\frac{\mathcal{E}_{\mathrm{b}}}{N_0}\right) = C(\gamma)\,, \tag{9}$$

with the value of γ provided by the solution to [28, Eq. (7)]

$$\frac{\mathcal{E}_{\mathrm{b}}}{N_0} = \frac{N_{\mathrm{T}}\, N_{\mathrm{R}}\gamma}{\mathbb{E}\left[\mathsf{Tr}\left\{\boldsymbol{H}^{\mathsf{H}}\boldsymbol{H}\right\}\right] C(\gamma)}\,.$$

According to [28], an affine expansion of the spectral efficiency of an $N_{\mathrm{R}} \times N_{\mathrm{T}}$ MIMO system, operating at low values of the transmitted SNR, can be obtained upon evaluation of the first- and second-order moment of the self-adjoint channel matrix $\boldsymbol{H}^{\mathsf{H}}\boldsymbol{H}$ as

$$\mathsf{C}\left(\frac{\mathcal{E}_{\mathrm{b}}}{N_0}\right) = \mathcal{S}_0\left(\frac{\mathcal{E}_{\mathrm{b}}}{N_0} - \left.\frac{\mathcal{E}_{\mathrm{b}}}{N_0}\right|_{\mathrm{min}}\right), \tag{10}$$

where

$$\mathcal{S}_0 = \frac{2N_{\mathrm{R}}}{\zeta\left(\boldsymbol{H}^{\mathsf{H}}\boldsymbol{H}\right)}\,, \tag{11}$$

$$\left.\frac{\mathcal{E}_{\mathrm{b}}}{N_0}\right|_{\mathrm{min}} = \frac{N_{\mathrm{T}}\log 2}{\mathbb{E}\left[\mathsf{Tr}\left\{\boldsymbol{H}^{\mathsf{H}}\boldsymbol{H}\right\}\right]}\,. \tag{12}$$

In (11), the term $\mathcal{S}_0$ (also referred to as low-power slope) depends on the so-called *dispersion* of the channel matrix which, for a square matrix $\boldsymbol{A}$ of size N, is defined as $\zeta(\boldsymbol{A}) = N\frac{\mathbb{E}[\mathsf{Tr}\{\boldsymbol{A}^2\}]}{\mathbb{E}^2[\mathsf{Tr}\{\boldsymbol{A}\}]}$.

The low-power behavior of (8) is fully captured by the following Proposition:

Proposition 4.1 *Given a mmWave MIMO channel as in (2), the low-power slope can be written as*

$$\mathcal{S}_0 = \frac{1}{N_{\mathrm{T}}} \frac{2N_{\mathrm{R}}L}{2 + \frac{L-1}{N_{\mathrm{R}}^2}\left(N_{\mathrm{R}} + \psi_{\mathrm{R}}\right) + \frac{L-1}{N_{\mathrm{T}}^2}\left(N_{\mathrm{T}} + \psi_{\mathrm{T}}\right)}, \tag{13}$$

where

$$\psi_{\mathrm{T}} = \sum_{h=1}^{N_{\mathrm{T}}} \sum_{h'=1, h' \neq h}^{N_{\mathrm{T}}} \mathbb{E}\left[\mathrm{e}^{\mathrm{j}\frac{2\pi d_{\mathrm{T}}}{\lambda}(h-h')\left(\cos\phi_{\mathrm{T},i} - \cos\phi_{\mathrm{T},j}\right)}\right]$$

and

$$\psi_{\mathrm{R}} = \sum_{h=1}^{N_{\mathrm{R}}} \sum_{h'=1, h' \neq h}^{N_{\mathrm{R}}} \mathbb{E}\left[\mathrm{e}^{\mathrm{j}\frac{2\pi d_{\mathrm{R}}}{\lambda}(h-h')\left(\cos\phi_{\mathrm{R},i} - \cos\phi_{\mathrm{R},j}\right)}\right].$$

Moreover, the term $\mathcal{E}_{\mathrm{b}}/N_0|_{\min}$ *is given by*

$$\left.\frac{\mathcal{E}_{\mathrm{b}}}{N_0}\right|_{\min} = \frac{\log 2}{N_{\mathrm{R}}}. \tag{14}$$

This result was obtained by particularizing (7) to $n = 1$ and $n = 2$. A detailed investigation of the low-power regime behavior of mmWave MIMO links requires the explicit evaluation of the phase-dependent parameters appearing at the denominator of $\mathcal{S}_0$. As a preliminary remark, we observe that for a single-input–single-output channel (*i.e.* for $N_{\mathrm{R}} = N_{\mathrm{T}} = 1$) with $L = 1$, $\mathcal{S}_0 = 1$. On the other hand, keeping the assumption of single-antenna equipped terminals, the expression of the low-power slope reduces to $\mathcal{S}_0 = \frac{1}{1+\frac{L-1}{2L}(\psi_{\mathrm{T}}+\psi_{\mathrm{R}})}$, and, by letting L grow unbounded, in turn, to $\mathcal{S}_0 = \frac{1}{1+\frac{(\psi_{\mathrm{T}}+\psi_{\mathrm{R}})}{2}}$.

4.2. High-SNR analysis

An affine expansion of the capacity for high SNR values can be written as (see [29] for details)

$$\mathcal{I}(\gamma) = \mathcal{S}_\infty(\gamma - \mathcal{L}_\infty),$$

where the high-SNR slope, $\mathcal{S}_\infty$, is given by the rank of $\boldsymbol{H}$. In our case, a typical assumption is to consider $L < \min\{N_{\mathrm{R}}, N_{\mathrm{T}}\}$ so that $\mathcal{S}_\infty = L$. The high-SNR power offset, $\mathcal{L}_\infty$, is given by [29, Formula (131)]

$$\mathcal{L}_\infty = \log_2 N_{\mathrm{T}} - \frac{1}{L}\mathbb{E}\log_2\left|\boldsymbol{H}^{\mathsf{H}}\boldsymbol{H}\right|.$$

Since $\boldsymbol{H} = \mathsf{g}\boldsymbol{U}\boldsymbol{D}\boldsymbol{V}^{\mathsf{H}}$, the term $\mathbb{E}\left[\log_2 |\boldsymbol{H}^{\mathsf{H}}\boldsymbol{H}|\right]$ can be rewritten as

$$\begin{aligned}\mathbb{E}\left[\log_2\left|\boldsymbol{H}^{\mathsf{H}}\boldsymbol{H}\right|\right] &= 2N_{\mathrm{T}}\log_2\mathsf{g} + L\mathbb{E}\log_2|\alpha|^2 \\ &\quad + \mathbb{E}\left[\log_2\left|\boldsymbol{V}^{\mathsf{H}}\boldsymbol{V}\right|\right] + \mathbb{E}\left[\log_2\left|\boldsymbol{U}^{\mathsf{H}}\boldsymbol{U}\right|\right].\end{aligned}$$

In particular, for the case $N_{\mathrm{R}} = N_{\mathrm{T}} = L$, one can write the high-SNR power offset in compact form hinging upon [22, Formula (17)], which leads to

$$\mathbb{E}\left[\log_2\left|\boldsymbol{V}\boldsymbol{V}^{\mathsf{H}}\right|\right] = L(L-1)\theta_{\mathrm{T}} - \log L, \tag{15}$$

$$\mathbb{E}\left[\log_2\left|\boldsymbol{U}\boldsymbol{U}^{\mathsf{H}}\right|\right] = L(L-1)\theta_{\mathrm{R}} - \log L, \tag{16}$$

where

$$\theta_{\mathrm{T}} = \mathbb{E}\left[\log\left|1 - \mathrm{e}^{\mathrm{j}kd_{\mathrm{T}}\left(\cos\phi_{\mathrm{T},i} - \cos\phi_{\mathrm{T},j}\right)}\right|\right]$$

and

$$\theta_{\mathrm{R}} = \mathbb{E}\left[\log\left|1 - \mathrm{e}^{\mathrm{j}kd_{\mathrm{R}}\left(\cos\phi_{\mathrm{R},i} - \cos\phi_{\mathrm{R},j}\right)}\right|\right].$$

5. Beyond linear array geometry

We will now describe how the geometric channel model in (2) can be represented when the transmitter and/or the receiver are equipped with array arrangements different from linear. In order to do so, we will provide new expressions of the transmit (or equivalently receive) steering vector $\boldsymbol{u}_\ell$ ($\boldsymbol{v}_\ell$). Without loss of generality, we omit the subscript ℓ in (3) indicating the path and we will refer to a generic steering vector $\boldsymbol{a}(\theta, \phi)$, where (θ, ϕ) is the Direction of Arrival (Departure), $\theta \in [0, \pi]$ is the elevation angle and $\phi \in [0, 2\pi]$ the azimuth.

The following array geometries are going to be considered:

1. Uniform Planar Array (UPA);
2. Uniform Circular Array (UCA);
3. Uniform Cylindrical Array (UCylA).

5.1. Uniform Planar Arrays

With reference to Fig. 2, we assume that the UPA [30] lies on the yz-plane (broadside to $\theta = \pi/2$, $\phi = 0$) with N_z antennas along the z-axis and N_y antennas along y-axis, $N = N_z N_y$. We can first write the $N_z \times 1$ steering vector of the ULA on z-axis $\boldsymbol{a}_z(\theta)$ with spacing d_z among antennas as

$$\boldsymbol{a}_z(\theta) = \left[1, \mathrm{e}^{\mathrm{j}kd_z\cos\theta}, \ldots, \mathrm{e}^{\mathrm{j}kd_z(N_z-1)\cos\theta}\right]^{\mathsf{T}}. \tag{17}$$

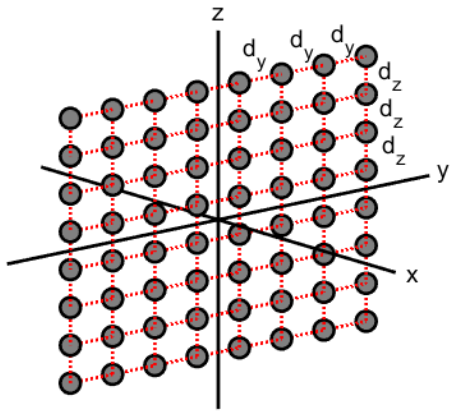

Fig. 2. Uniform Planar Array.

Secondly, we denote with $\boldsymbol{a}_y(\theta,\phi)$ the $N_y \times 1$ the steering vector of the ULA that lies on the y-axis with spacing d_y

$$\boldsymbol{a}_y(\theta,\phi) = \left[1, \mathrm{e}^{\mathrm{j}kd_y \sin\theta \sin\phi}, \ldots, \mathrm{e}^{\mathrm{j}kd_y(N_y-1)\sin\theta\sin\phi}\right]^{\mathsf{T}} . \tag{18}$$

Then, we define the $N_z \times N_y$ array manifold matrix $\mathbf{A}_{\mathrm{UPA}} = \boldsymbol{a}_z(\theta)\boldsymbol{a}_y^{\mathsf{T}}(\theta,\phi)$

$$\mathbf{A}_{\mathrm{UPA}} = \begin{bmatrix} 1 & \ldots & \mathrm{e}^{\mathrm{j}kd_y(N_y-1)\sin\theta\sin\phi} \\ \vdots & \ddots & \vdots \\ \mathrm{e}^{\mathrm{j}kd_z(N_z-1)\cos\theta} & \ldots & \mathrm{e}^{\mathrm{j}k[d_z(N_z-1)\cos\theta + d_y(N_y-1)\sin\theta\sin\phi]} \end{bmatrix} . \tag{19}$$

Finally, the $N \times 1$ steering vector $\mathbf{a}_{\mathrm{UPA}}(\theta,\phi)$ can be expressed as

$$\mathbf{a}_{\mathrm{UPA}}(\theta,\phi) = \mathrm{vec}\left(\mathbf{A}_{\mathrm{UPA}}^{\mathsf{T}}\right) , \tag{20}$$

where $\mathrm{vec}(\cdot)$ indicates the vectorization of a matrix. If the transmitter (or equivalently the receiver) is equipped with a UPA, we can therefore redefine $\boldsymbol{U}$ (or $\boldsymbol{V}$) in (2) as

$$\boldsymbol{U} = [\boldsymbol{a}_{\mathrm{UPA}}(\theta_1,\phi_1), \ldots, \boldsymbol{a}_{\mathrm{UPA}}(\theta_l,\phi_l), \ldots, \boldsymbol{a}_{\mathrm{UPA}}(\theta_L,\phi_L)] , \tag{21}$$

where (θ_l,ϕ_l) indicates the Direction of Departure (Arrival) corresponding to the ℓ-path.

5.2. Uniform Circular Array

For the case of the circular array [30, 31], we assume that the UCA lies in the xy-plane as shown in Fig. 3 with N_{c} antennas and radius R. Antennas

are then spaced $\frac{2\pi R}{N_c}$ along the arc. The corresponding $N_c \times 1$ steering vector $\boldsymbol{a}_{\mathrm{UCA}}(\theta, \phi)$ can be expressed as

$$\boldsymbol{a}_{\mathrm{UCA}}(\theta,\phi) = \left[\mathrm{e}^{\mathrm{j}kR\sin\theta\cos\phi}, \mathrm{e}^{\mathrm{j}kR\sin\theta\cos\left(\phi-\frac{2\pi}{N_c}\right)}, \ldots, \mathrm{e}^{\mathrm{j}kR\sin\theta\cos\left(\phi-2\pi\frac{N_c-1}{N_c}\right)}\right]^{\mathsf{T}}. \tag{22}$$

It can be noted that if the steering vector $\boldsymbol{u}_\ell$ ($\boldsymbol{v}_\ell$) is defined as in (22), then $\boldsymbol{U} = [\boldsymbol{a}_{\mathrm{UCA}}(\theta_1, \phi_1), \ldots, \boldsymbol{a}_{\mathrm{UCA}}(\theta_L, \phi_L)]$ is a generalized Vandermorde matrix [11].

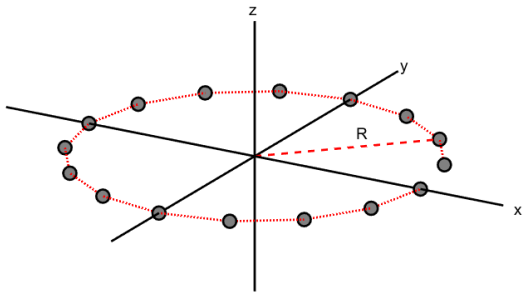

Fig. 3. Uniform Circular Array.

5.3. Uniform Cylindrical Array

By stacking multiple UCAs along z, we can form a cylindrical array [31–33], as shown in Fig. 4. The UCylA is made of N_z horizontal ring subarrays with radius R, spaced vertically d_z, and with N_c elements per ring, $N = N_c N_z$. Let us define the $N_z \times 1$ steering vector of the ULA lying on the z-axis

$$\boldsymbol{a}_{\mathrm{ULA}}(\theta) = \left[\mathrm{e}^{-\mathrm{j}kd_z\frac{N_z-1}{2}\cos\theta}, \ldots, \mathrm{e}^{\mathrm{j}kd_z\frac{N_z-1}{2}\cos\theta}\right]^{\mathsf{T}}, \tag{23}$$

where the difference with respect to (17) of the planar case is the phase reference point, which is the center of the cylinder. We define the $N_z \times N_c$ array manifold matrix $\mathbf{A}_{\mathrm{UCylA}} = \boldsymbol{a}_{\mathrm{ULA}}(\theta)\boldsymbol{a}^{\mathsf{T}}_{\mathrm{UCA}}(\theta, \phi)$

$$\mathbf{A}_{\mathrm{UCylA}} = \begin{bmatrix} \mathrm{e}^{\mathrm{j}k\left[R\sin\theta\cos\phi - d_z\frac{N_z-1}{2}\cos\theta\right]} & \cdots & \mathrm{e}^{\mathrm{j}k\left[R\sin\theta\cos\left(\phi-2\pi\frac{N_c-1}{N_c}\right) - d_z\frac{N_z-1}{2}\cos\theta\right]} \\ \vdots & \ddots & \vdots \\ \mathrm{e}^{\mathrm{j}k\left[R\sin\theta\cos\phi + d_z\frac{N_z-1}{2}\cos\theta\right]} & \cdots & \mathrm{e}^{\mathrm{j}k\left[R\sin\theta\cos\left(\phi-2\pi\frac{N_c-1}{N_c}\right) + d_z\frac{N_z-1}{2}\cos\theta\right]} \end{bmatrix}. \tag{24}$$

In the same way as (20), the final $N \times 1$ steering vector $\boldsymbol{a}_{\mathrm{UCylA}}(\theta, \phi)$ is equal to $\mathrm{vec}(\mathbf{A}^T_{\mathrm{UCylA}})$. Therefore, $\boldsymbol{U} = [\boldsymbol{a}_{\mathrm{UCylA}}(\theta_1, \phi_1), \ldots, \boldsymbol{a}_{\mathrm{UCylA}}(\theta_L, \phi_L)]$, and similarly to the UCA case, $\boldsymbol{U}$ is a generalized Vandermorde matrix.

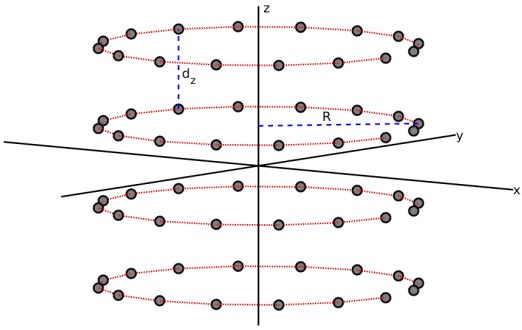

Fig. 4. Uniform Cylindrical Array.

6. Conclusion

Given the relevance of random matrices in the modeling mmWave MIMO channels, we reported some interesting results that are available in the literature and that can be readily used for the performance analysis of 5G and beyond communication systems. We started by highlighting the need for novel tools to model mmWave links, then we observed that mmWave MIMO channel can be represented as a mixed product of random Vandermonde matrices and random diagonal matrices. We underlined the open issues and emphasized the impact of different antenna array geometries on the structure of the matrices modeling the channel.

REFERENCES

[1] I.E. Telatar, «Capacity of multi-antenna Gaussian channels», AT&T Bell Laboratories Technical Report, BL0112170-950615-07TM, June 1995.

[2] R.R. Müller, *IEEE Trans. Inform. Theory* **48**, 2086 (2002).

[3] A. Tulino, S. Verdú, «Random Matrix Theory and Wireless Communications», *Foundations and Trends in Communications and Information Theory*, 2004, Vol. 1.

[4] R. Couillet, M. Debbah, «Random Matrix Methods for Wireless Communications», *Cambridge University Press*, Cambridge 2011.

[5] G. Akemann, J. Baik, P. Di Francesco (Eds.) «The Oxford Handbook of Random Matrix Theory», *Oxford University Press*, 2011.

[6] R. Müller, G. Alfano, B.M. Zaidel, R. de Miguel, arXiv:1310.5479 [cs.IT].

[7] N. Fawaz, K. Zarifi, M. Debbah, D. Gesbert, *IEEE Trans. Inform. Theory* **57**, 2050 (2011).

[8] G.F. Pivaro, S. Kumar, G. Fraidenraich, C.F. Dias, *IEEE Trans. Veh. Technol.* **66**, 10537 (2017).

[9] J.G. Andrews *et al.*, *IEEE J. Sel. Areas Commun.* **32**, 1065 (2014).
[10] X. Song, S. Haghighatshoar, G. Caire, *IEEE Trans. Wireless Commun.* **17**, 4792 (2018).
[11] Ø. Ryan, M. Debbah, *IEEE Trans. Inform. Theory* **55**, 3115 (2009).
[12] V. Raghavan *et al.*, *IEEE J. Sel. Top. Signal Process.* **10**, 543 (2016).
[13] A.A.M. Saleh, R. Valenzuela, *IEEE J. Sel. Areas Commun.* **5**, 128 (1987).
[14] Z. Zheng, H. Gharavi, *IEEE Trans. Veh. Technol.* **68**, 5732 (2019).
[15] M.R. Akdeniz *et al.*, *IEEE J. Sel. Areas Commun.* **32**, 1164 (2014).
[16] S. Buzzi, C. D'Andrea, arXiv:1604.00648 [cs.IT].
[17] A. Nordio, C.-F. Chiasserini, E. Viterbo, *IEEE Trans. Signal Process.* **56**, 4274 (2008).
[18] A. Nordio, C.-F. Chiasserini, E. Viterbo, *IEEE Trans. Signal Process.* **56**, 3535 (2008).
[19] A. Nordio, G. Alfano, C.-F. Chiasserini, A.M. Tulino, *IEEE Trans. Signal Process.* **59**, 2760 (2011).
[20] G.H. Tucci, P.A. Whiting, *IEEE Trans. Inform. Theory* **57**, 3938 (2011).
[21] I. Reed, *IRE Trans. Inform. Theory* **8**, 194 (1962).
[22] G.H. Tucci, P.A. Whiting, *J. Theor. Probab.* **27**, 826 (2014).
[23] B. Au, Gu. Cébron, A. Dahlqvist, F. Gabriel, C. Male, arXiv:1805.07045 [math.PR].
[24] M. Boedihardjo, K. Dykema, *Adv. Math.* **318**, 1 (2017).
[25] C. Male, arXiv:1111.4662 [math.PR].
[26] G.W. Anderson, B. Farrell, *Adv. Math.* **255**, 381 (2014).
[27] A.M. Tulino, G. Caire, S. Shamai, S. Verdú, *IEEE Trans. Inform. Theory* **56**, 1187 (2010).
[28] A. Lozano, A. Tulino, S. Verdú, *IEEE Trans. Inform. Theory* **49**, 2527 (2003).
[29] A. Lozano, A.M. Tulino, S. Verdu, *IEEE Trans. Inform. Theory* **51**, 4134 (2005).
[30] C.A. Balanis, «Antenna Theory: Analysis and Design», *Wiley-Interscience*, 2005.
[31] H.L. Van Trees, «Optimum Array Processing: Part IV of Detection, Estimation, and Modulation Theory», *John Wiley & Sons*, 2004.
[32] D.G. Riviello, R. Garello, «Implementation of 5G beamforming techniques on cylindrical arrays», 2019 IEEE-APS Topical Conference on Antennas and Propagation in Wireless Communications (APWC), Granada, Spain, 2019, pp. 413–418.
[33] D.G. Riviello, F. Di Stasio, «5G beamforming implementation and trade-off investigation of cylindrical array arrangements», 2019 22nd International Symposium on Wireless Personal Multimedia Communications (WPMC), Lisbon, Portugal, 2019, pp. 1–6.